13

Using Optical Coherence Tomography to Characterize the Crack Morphology of Ceramic Glaze and Jade

M.-L. Yang, A.M. Winkler, J. Klein, A. Wall and J.K. Barton
Tamkang University, Taipei, Taiwan

1. Introduction

The utilization of optical coherence tomography (OCT) in artworks' examination for the past several years has confirmed its feasibility (Elias et al., 2010; Targowski, 2008). The results not only aid authentication of museum collections, but also provide crucial information for understanding artworks' manufacturing technology and use history, as well as for continuing preservation. To display certain characteristics of ceramic glaze and jade materials, such as components assemblage, bubbles distribution, glaze-layer structure, cracks morphology and alteration phenomenon, OCT is an ideal tool. In previous research, the bubble distribution and components assemblage within Chinese glaze samples has been discussed (Yang et al., 2011, 2009), and the alteration of archaic jade has also been examined (Liang et al., 2008; Yang et al., 2004). In addition, with specific algorithm programs, the researcher is also able to obtain quantitative data, such as the bubble size and number in a glaze or intensities of texture vector in a jade material (Klein et al., 2011; Chang et al., 2010).

In the present chapter, various cracks' morphology in Chinese glaze and jade samples are described and characterized using OCT systems. Cracks are common in brittle materials, such as traditional glass, ceramics, or even tougher semi-gem or rock. In general, they are regarded as defective in artistic or industrial products. However, certain cracks were endowed with an artistic or cultural attribute or significance because of their special morphology and uniquely formed patterns. Moreover, they were surmised to be intentionally created, such as Chinese Song Dynasty (AD 960-1279) Ru and Guan wares. They were made by contemporary imperial potters and possessed a high density and diversity of crack patterns. Therefore, determining morphology and characteristics of cracks in glaze and jade artifacts would not only contribute to scientific ceramics and jade research, but also benefit art history study.

2. OCT systems and samples properties

Cracks in jade or glaze, translucent or somewhat transparent materials, can be viewed by the naked eye or observed on the surface of the artifact under a microscope at low magnification. Then, for accurate examination of their structure, the destructive thin section

method, or scanning electron fractography, has been used for the past several decades (Friedman et al., 1972; Coppola & Bradt, 1972). However, the present OCT systems not only provide a non-destructive, rapid technique for presenting crack morphology in a two-dimension or even three-dimension image in cross section, and also yield abundant information about the relationship between cracks and local components.

2.1 Three OCT systems

Three different OCT systems were utilized for this study, in order to meet different research objectives. The systems have varying wavelengths, resolution and sensitivity to features in the glaze and jade samples. The chosen system presents the optimal image resolution of crack and their matrix. The first OCT system was a commercial system equipped with a handheld probe, a Thorlabs Spectral Radar OCT system (THORLABS, 2011). This system uses a central wavelength of 930-nm and a spectrum width of nearly 100-nm as its light source, resulting in an image resolution in axial resolution approximately 6.0-μm and the lateral resolution approximately 9.0-μm. This system presents a clear crack structure in complicated microstructure glaze samples.

The second OCT system was custom built (Winkler et al., 2010). The light source is a superluminescent diode (Superlum Broadlighter, Moscow, Russia) with an 890-nm center wavelength and a 150-nm bandwidth that results in an image resolution better than 3.0-μm axial and 5-μm lateral, in glaze or jade. This system provides the most optimal crack structure images for most jade (nephrite) samples in a depth of over 1-mm.

The third system was also custom built. It is a focus-tracking OCT system. Its light source (Superlum Broadlighter 855) features 100-nm in bandwidth with a center wavelength of 855-nm, that, when coupled with a moderate numerical aperture objective, permits a 4-5.0-μm isotropic imaging resolution. The benefit of this system is that it optimally maintains lateral resolution at all depths within a sample having a refractive index of ~1.4 (Yang et al., 2011). For the present research, to image sealed cracks located in a deeper position from the sample's surface, this system is a powerful tool.

2.2 Glaze material and crack types

Three primary phases (components): homogeneous glass phase, crystallization phase, and liquid-liquid phase separation, with a few un-melted quartz or residuals particles, are usually contained in traditional Chinese glazes in a multi-phase assemblage or single phase dominant states. However, for the feldspar glaze used in Chinese celadon, the crystallization phase is usually formed by anorthite ($CaO \cdot Al_2O_3 \cdot 2SiO_2$) and wollastonite (or pseudowollastonite $CaO \cdot SiO_2$) (Yang et al., 2009; Kingery et al., 1976).

These phases (components) are displayed in nuanced gray scale in the OCT image based on the relative difference of their individual refractive index (n) as the homogeneous glass n = 1.5, then, wollastonite n_α = 1.616 - 1.640, n_β = 1.628 - 1.650, n_γ = 1.631 - 1.653, anorthite n_α = 1.577, n_β = 1.585, n_γ = 1.590 and quartz n_ω = 1.544, n_ε = 1.553. At times, a few iron oxides are formed in the glaze, such as hematite (Fe_2O_3, n_ω = 3.22, n_ε = 2.94). In addition, the liquid-liquid phase separation is in a somewhat different refractive index from the homogeneous glass phase (Simmons, 1977). The relevant optical properties and OCT image expression of

these components within Chinese glaze was introduced in a previous publication (Yang et al., 2009).

Two classes of cracks occurring in glaze are usually mentioned: one caused by thermal shock when the ceramic product is removed from the kiln; the other caused by moisture on porcelain or pottery bodies during storage or use (Shaw, 1971; Norton, 1952; Schurecht & Fuller, 1931). The latter is also called 'delayed crazing.' Actually, the former is the primary crazing on all glazed ceramics. In the past, some researchers categorized crack morphology into a few types based on surface viewing (Faber et al., 1981; Schurecht & Pole, 1932; Schurecht & Fuller, 1931; Gao, 1591). However, viewing the cross section from the surface to the interior glaze or body seems to simplify all crack morphology types to a single one, a 'T' structure with various inclining angles in 'I', that represent the crack path basically in a vertical direction from the surface of the glaze, and '—' representing the horizontal direction of the surface. In addition, we kept all samples in a horizontal position during scanning.

Crack presentation in an OCT image should theoretically be a bright (white), linear structure, because it is actually a narrow gap (air) or a boundary between two displaced faces. However, the brightness of the crack line partly depends on local components and texture. In addition to the thermal stress within a glaze, the glaze's features, such as components' species, micro-structure, even bubbles' distribution, impurity grains' size, among others, also influence crack morphology (Seaton & Dutta, 1974; Coppola & Bradt, 1972; Hasselman, 1969; Coble & Kingery, 1955). Three different features of celadon glaze samples are examined to describe the variation in crack structure. The glaze samples' descriptions are listed in Table 1.

2.3 Jade material and crack types

Two primary minerals, nephrite and jadeite are used as jade material in China. The former was always highly valued by the ancient Chinese, and used for fashioning ritual and ceremonial objects or even utility tools in the very early stage, the Neolithic period (5000-2000 BCE). In contrast, the latter was used very late, around the middle of the eighteenth century (Palmer, 1967; Whitlock & Ehrmann, 1949). Nephrite possesses considerable toughness and strength because of its compact fibrous crystalline structure, permitting considerable mechanic stress during the fashioning or mining process (Bradt et al., 1973).

According to ancient Chinese texts, cracks in jade materials were usually described by various terms based on visible features, such as '*liu(綹)*,' '*wen(璺)*'or '*dian(玷)*' (Gao, 1591; Li, 1925), but, respectively, they were not defined clearly. However, based on cross section viewing in OCT images, two basic types of crack in jade materials are the linear structure open to the air, usually with brown corrosion (iron oxidation) along its path, and the cloudy clustering structure sealed off from the surface in a deeper position inside the jade material.

However, because of its compact crystalline structure and a refractive index n=1.606-1.632, a pure nephrite's matrix is displayed in OCT image to be very simple and even light gray scale (Yang et al., 2004). Then, regardless of the linear or clustering structure cracks in jade (nephrite), because most cracks propagate along the boundary of the grains in a jade material, the crack path is revealed somewhat irregularly or zigzag. Four jade (nephrite) samples are examined, as described in Table 1.

sample #	thickness/mm	material	date	form	provenance
glaze-1	~0.7	feldspar glaze	10-13th century	shard	Hangzhou, Zhejiang
glaze-2	~0.7	feldspar glaze	10-13th century	shard	Hangzhou, Zhejiang
glaze-3	~0.5	feldspar glaze	10th century	shard	Chinglianssu, Henan
jade-1	0.2-0.25	nephrite	~2500 BCE	huang-arch	Gansu
jade-2	0.5-0.6	nephrite	~2500 BCE	adze (broken)	Shaanxi
jade-3*	~0.4	nephrite	~2500 BCE	huang-arch	Gansu
jade-4**	-	nephrite	-	natural pebble	Xinjiang

* jade-3 in the author's original samples collection number is jade-12.
** jade-4 in the author's original samples collection number is jade-7.

Table 1. Samples' descriptions.

3. Characterizing crack morphology in glaze

The three crucial characteristics of crack morphology in the glaze, its opening on the surface, structure and terminal tip in the matrix, and its relationship with local components, are discussed below.

3.1 Cracks in a homogeneous glass phase dominant glaze

Figure 1a presents a crack in a homogeneous glass phase dominant glaze, sample glaze-1, with several bubbles (pairing bright dots). The crack morphology is a typical 'T' structure in cross section. A small chip reveals its opening on the surface of the glaze. In the OCT image, with an increased scanning depth, the crack resembles an upside down cone hanging from the surface, explaining the scattering signals' gradual weakening by crack surrounding components. However, along the crack path, two larger impurity grains are revealed. The upper one is surmised to influence the crack's continuing direction, and the lower one to terminate this crack.

Three cracks are presented in Figure 1b. The right crack is large with two chips at its opening. This crack displays a typical 'T' structure with a slight incline to the right. The tip of crack seems to terminate at an impurity grain (lower arrow) just below the tip. The 'T' structure crack is similar to the crack in a modern blown glass fragment (Figure 2). Thus, a reasonable conclusion seems to be that in a homogeneous glass phase dominant glaze, a crack usually propagates in a typical 'T' structure with a slight incline.

In addition, in Figure 1b, on the left, next to the large right crack, two thin crack lines are displayed. One is long, propagating at an inclining angle of around 30 degrees to the left, and terminating in the interface area between the glaze and body. The other is short and probably terminated at the long crack gap. However, the openings of the two thin cracks are not revealed clearly on the surface.

The image in Figure 1c clearly presents two cracks and another vague crack behind the left crack. The right one is almost a typical 'T' structure with a slight incline to the right, terminating at an impurity grain just below its tip. No chip is revealed at its opening on the

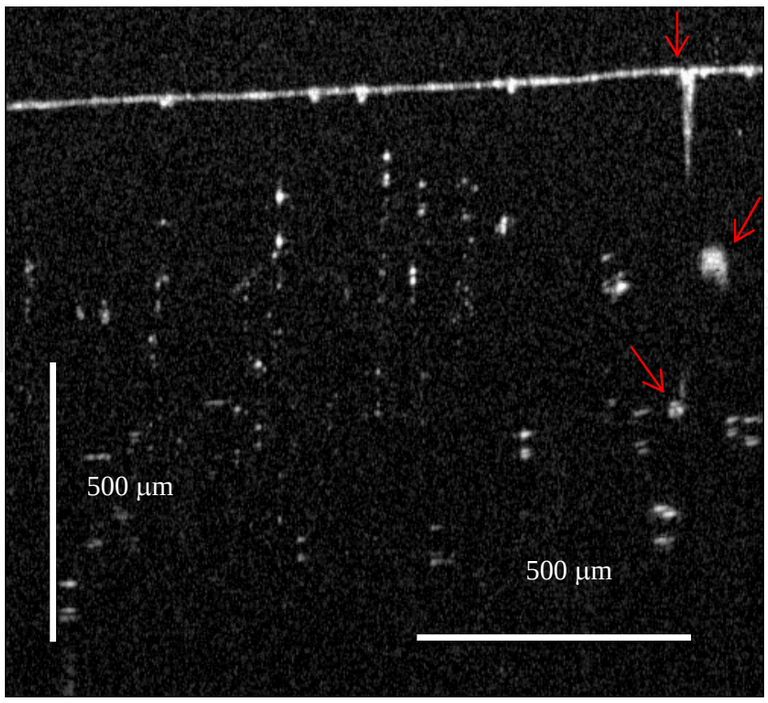

Fig. 1a. A typical 'T' structure crack is presented in the sample glaze-1 (upper arrow). A chip reveals its opening on the surface, and below the tip of crack two impurities grains (middle and lower arrows) probably governed its path. (image acquired by 930-nm system).

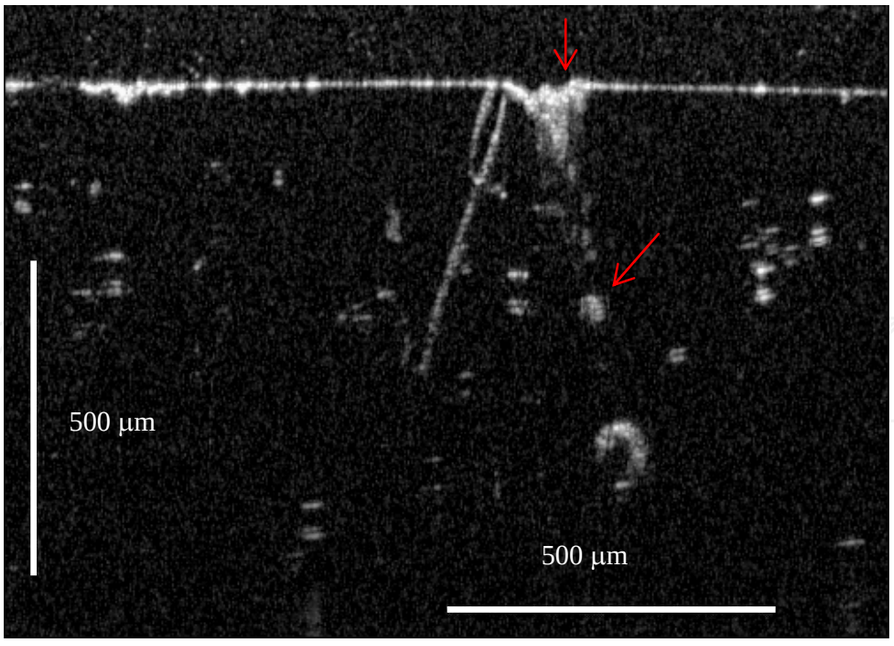

Fig. 1b. The right arrow points to a large 'T' structure crack with a slight incline to the right. Two big chips are at its opening, and the crack is probably terminated at an impurity grain (lower arrow). The left two cracks, one long and the other short are almost parallel and incline to the left at around 30 degrees. (image acquired by 930-nm system).

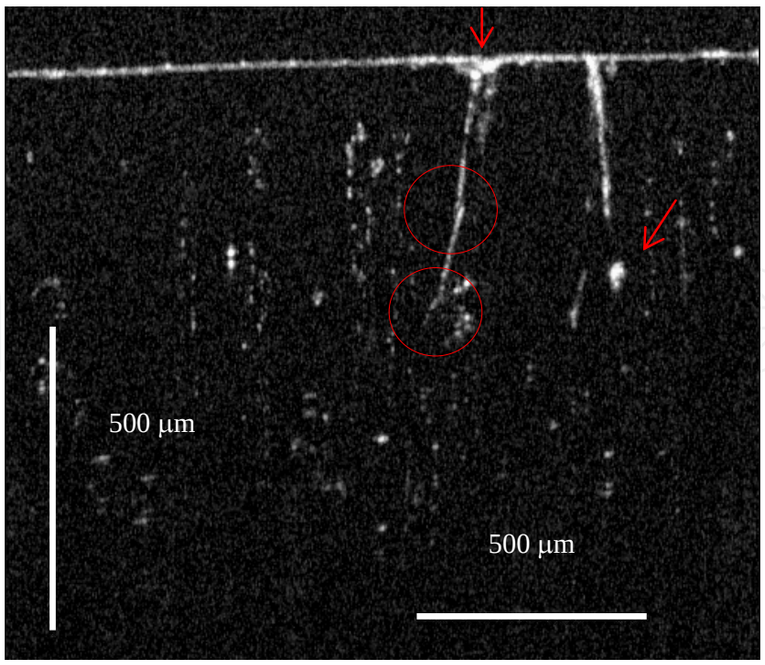

Fig. 1c. The right crack is almost a typical 'T' structure with a slight incline to the right, and terminates at an impurity grain just below its tip (lower arrow). The left crack seems to transfer its path at two positions (circles). In addition, a vague crack is revealed behind the left crack. (image acquired by 930-nm system).

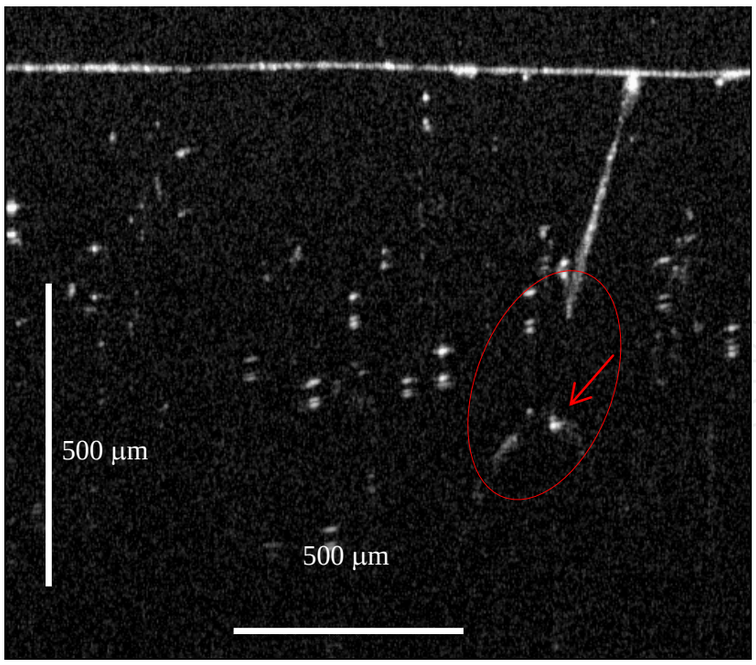

Fig. 1d. A crack inclines to the left at around 30 degrees. This crack probably transferred its path at a position (circle) further to the left as it encountered an impurity grain (arrow). (image acquired by 930-nm system).

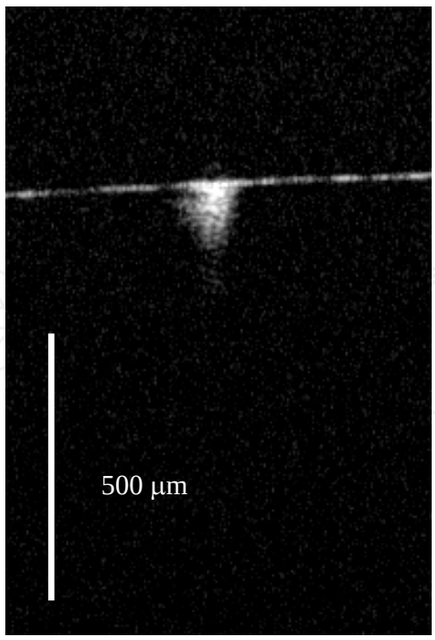

Fig. 2. A typical 'T' structure crack in a homogeneous blown glass fragment. (image acquired by 930-nm system).

surface. In contrast, the left one displays its opening chip and path that inclines somewhat to the left. However, its path transfers at two positions (upper and lower circles), around 0.3-mm and 0.5-mm in depth from the surface.

A crack in Figure 1d is similar to the left crack structure in Figure 1c. This crack probably diverged from the original path more to the left at the interface area between the glaze and body, around 0.7-mm in depth from the surface, as the crack encountered an impurity grain (arrow). Then, it continued to propagate into the body where it diminished. The opening is not open to the air.

3.2 Cracks in a multi-phase inhomogeneous glaze

Figure 3a presents a somewhat complicated phases' assemblage in the sample glaze-2. The black portion and various gray scale portions entangled and assembled into a multi-phase inhomogeneous glaze texture with several bubbles. Two cracks are presented in this image. The right one is large with a broad chip at the opening on the surface, and is characterized as a typical 'T' structure crack. The left crack's path is not clearly revealed at this scanning position, but its chip at the opening is clearly revealed. However, a large impurity grain (lower arrow) surrounding it probably governed this crack's path.

Figure 3b presents three cracks in a somewhat tight space. The central one is a 'T' structure crack with a slight incline to the left. The left one (left arrow) propagated its path into two sides in almost same inclining angle, around 60 degrees. It appears to be apparent that this crack propagated in a shallower position from the surface of the glaze. The right one (right arrow) is not displayed clearly at this scanning position. However, its structure seems similar to the left crack.

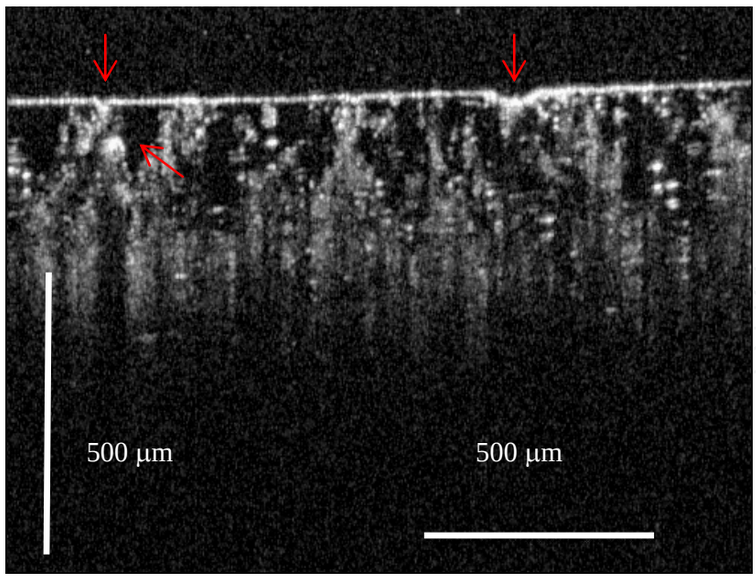

Fig. 3a. The right crack is a typical 'T' structure with big chip at its opening on the surface. The left crack path is not clearly presented at this scanning position, but the chip of its opening (left upper arrow) is clearly revealed. The impurity grain (lower arrow) probably influenced this crack path. (image acquired by 930-nm system)

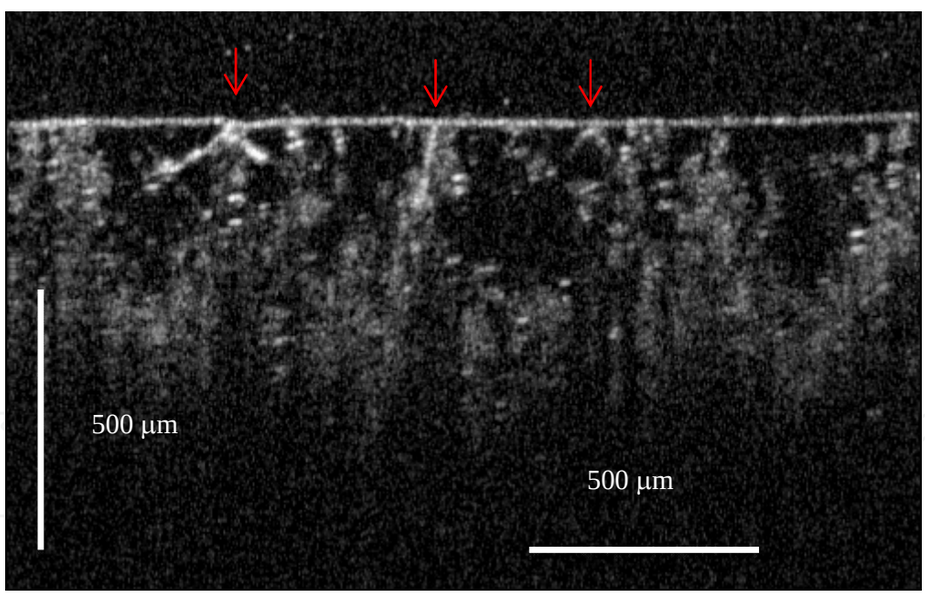

Fig. 3b. The left crack separated into left and right paths. A large inclining angle, around 60 degrees, propagated the crack path in a shallower position from the surface. The central crack is a typical 'T' structure with a slight incline to the left. The right crack is not clearly visualized at this scanning position. (image acquired by 930-nm system)

A crack that propagates in a shallower position from the surface creates a specific visual effect. Figure 4 displays several cracks in a tight space with a nuanced visual effect in the microphotograph of the sample glaze-3. However, the primary distinction among these

cracks lies in their inclining angles. It appears to be apparent that the larger the inclining angle, the shallower the crack propagates. It causes a cloudy visual effect in the texture of the crack's range. In contrast, the smaller the inclining angle, the deeper the crack propagates almost vertically penetrating to the interior glaze and usually without changing the original visual effect in the local texture.

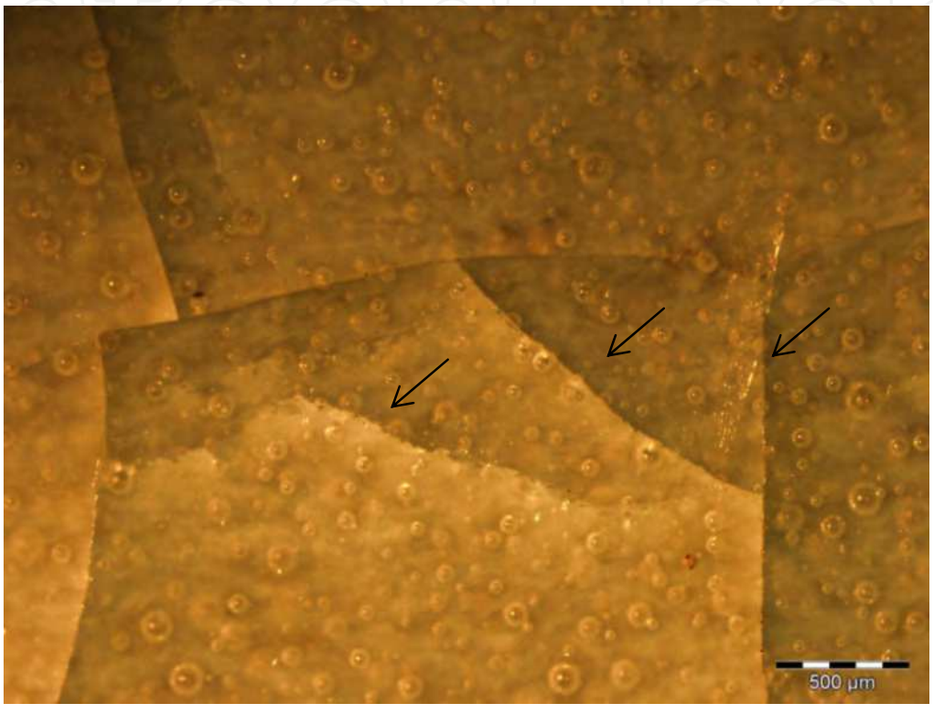

Fig. 4. The microphotograph of the sample glaze-3 presents several cracks in the tight space. Three arrows point to three different visual effect cracks. The lower crack (left arrow) presents cloudy texture, whereas the right crack (right arrow) is close to original translucent glaze quality.

Comparing with the glaze-2, the sample glaze-3 is a more structural multi-phase inhomogeneous glaze with a richer gray portion. According to our previous research on glaze-3, it consists of homogeneous glass phase, crystallization phase (anorthite and pseudowollastonite) and liquid-liquid phase separation (Yang et al., 2009). Two cracks are presented in images in Figure 4a (including Figure 4a-1 and 4a-2). The right crack is characterized as a 'T' structure with an inclining angle around 30 degrees and terminated at a bubble (Figure 4a-2; lower arrow). The chip of its opening is revealed on the surface. However, the left crack seems to somewhat bend its path slightly to the left.

Figure 4b displays a very shallow crack which propagated its path in an almost horizontal direction to the right, and terminated at a bubble. This shallow crack appears in a disconnected path based on the OCT image. It meets the lower crack (Figure 4; left arrow) in the microphotograph that exhibits a considerable cloudy visual effect in this crack range.

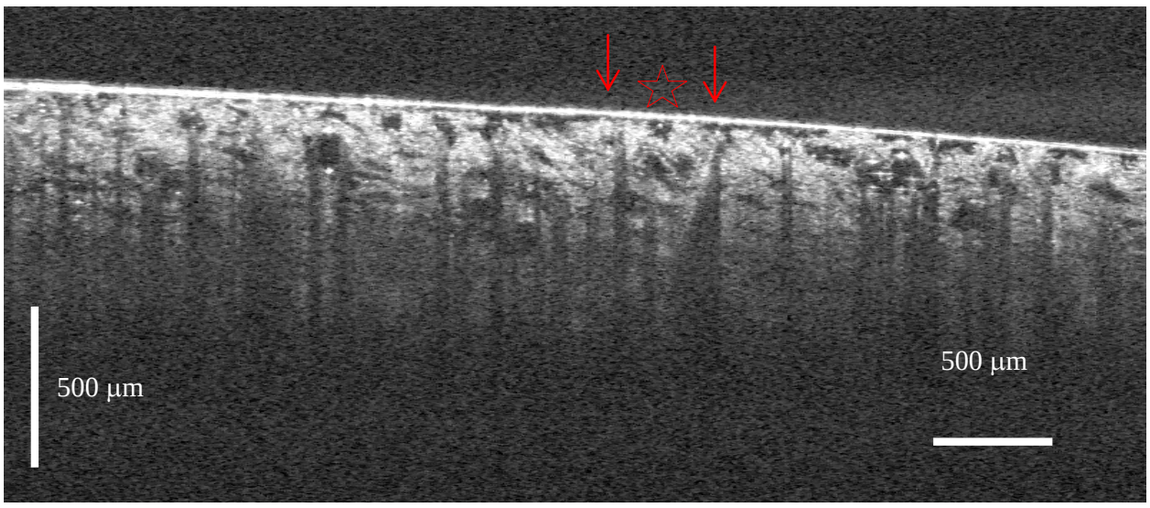

Fig. 4a. A multi-phase inhomogeneous glaze is in tight compact structure, and two cracks are revealed (two arrows; the star is a landmark in the sample glaze-3). (image acquired by 890-nm system).

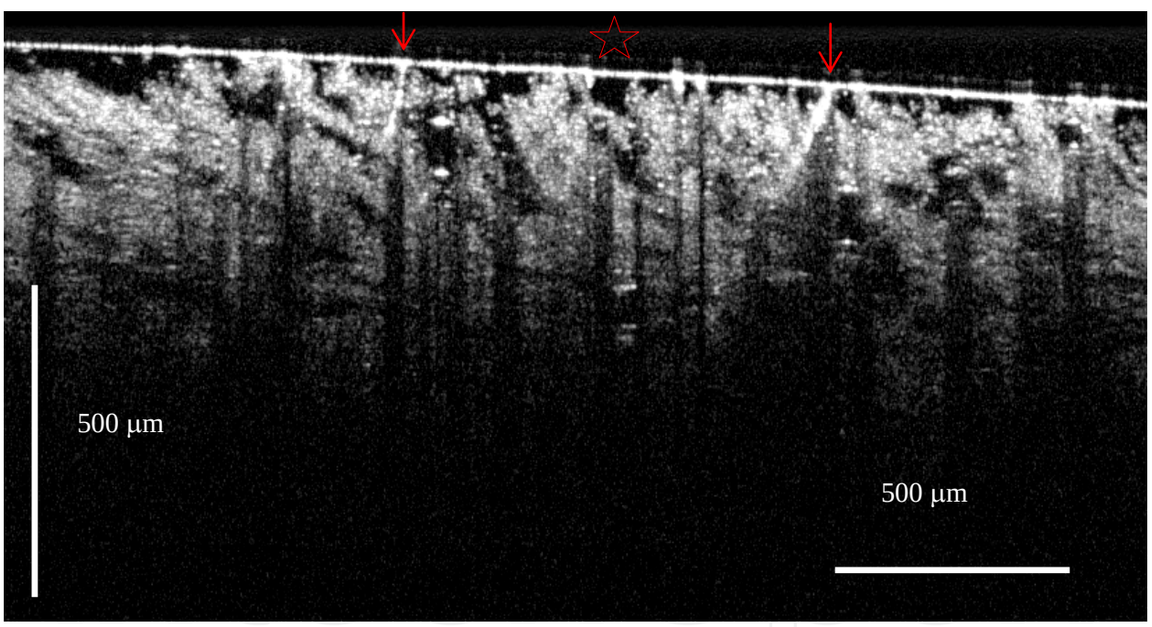

Fig. 4a-1. The right crack is apparently inclining to the left around 45 degrees, whereas the left inclines slight to the left. The former reveals a partially clear chip at its opening. (image acquired by 930-nm system).

3.3 Discussion of the characteristics of crack morphology in glaze

For a homogeneous glass dominant glaze, the characteristics of crack morphology are concluded as: (1) some cracks are not open to the air; (2) crack structure is basically presented in a 'T' structure with a slight incline; (3) most cracks are terminated at larger impurity grain or bubble located just below the tip of the crack; and, (4) some cracks probably diverge from their original path when they encounter grain impurities.

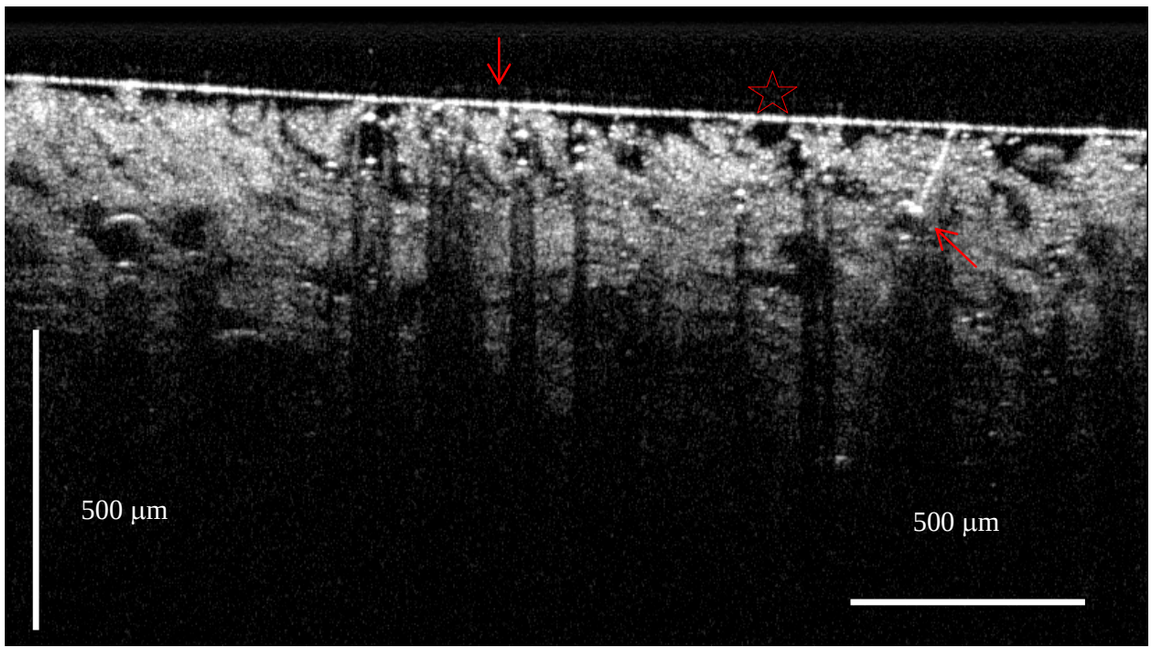

Fig. 4a-2. The right crack is terminated at a bubble. The left crack is not clearly revealed at this scanning position (image acquired by 930-nm system).

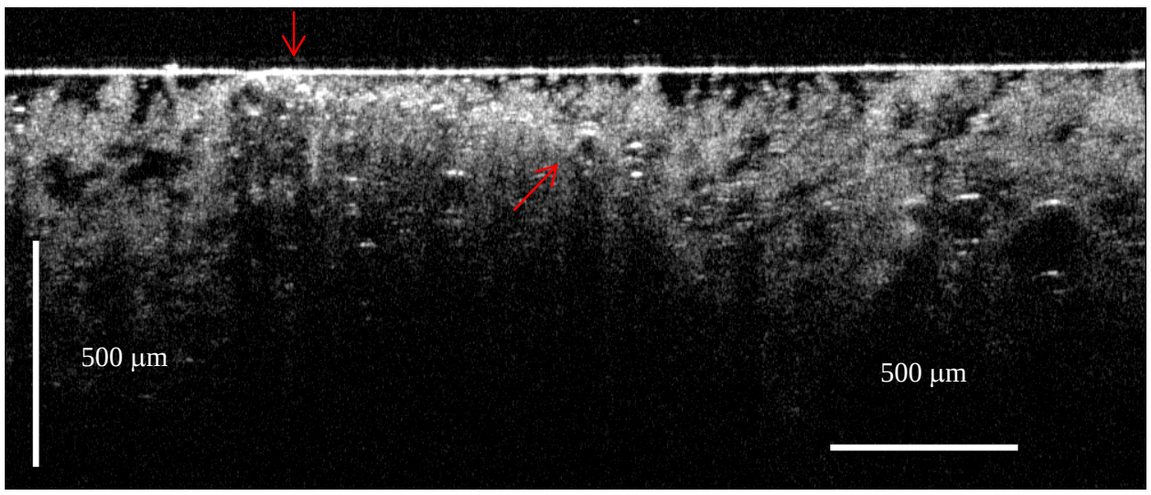

Fig. 4b. A crack appears in very shallow position from the surface that propagated in disconnected and horizontal path, and terminated at a bubble. (image acquired by 930-nm system).

Most of the characteristics of cracks in a multi-phase inhomogeneous glaze are the same as those in the homogeneous glass dominant glaze. However, because the inclining angle variation is richer and more nuanced in the former, it appears to create a higher diversity and higher density of crack patterns. Moreover, it also achieves a subtle visual effect in the texture of the crack range.

4. Characterizing crack morphology in jade

Compared with the considerable diversity of gray scale in the OCT images of a multi-phase inhomogeneous glaze, in addition to lacking bubbles, the jade's OCT images are quite simple and even. As formerly mentioned, the two basic types of crack in jade are clustering and linear structure.

4.1 Clustering structure crack in jade

Figure 5 is a microphotograph of the sample jade-1, presenting several clustering cracks in the cloudy clusters, most of them sealed below the surface in various depths, whereas a few micro-cracks are open to the air in a few bright sparks within the circle. Figure 5a presents two clustering structure cracks in the image. The left one reveals that it consisted of many micro-cracks and propagated into a considerable volume. The right one is not clearly presenting its clustering structure at this scanning position, but it reveals a few chips on the surface, and damage to the texture of the local matrix.

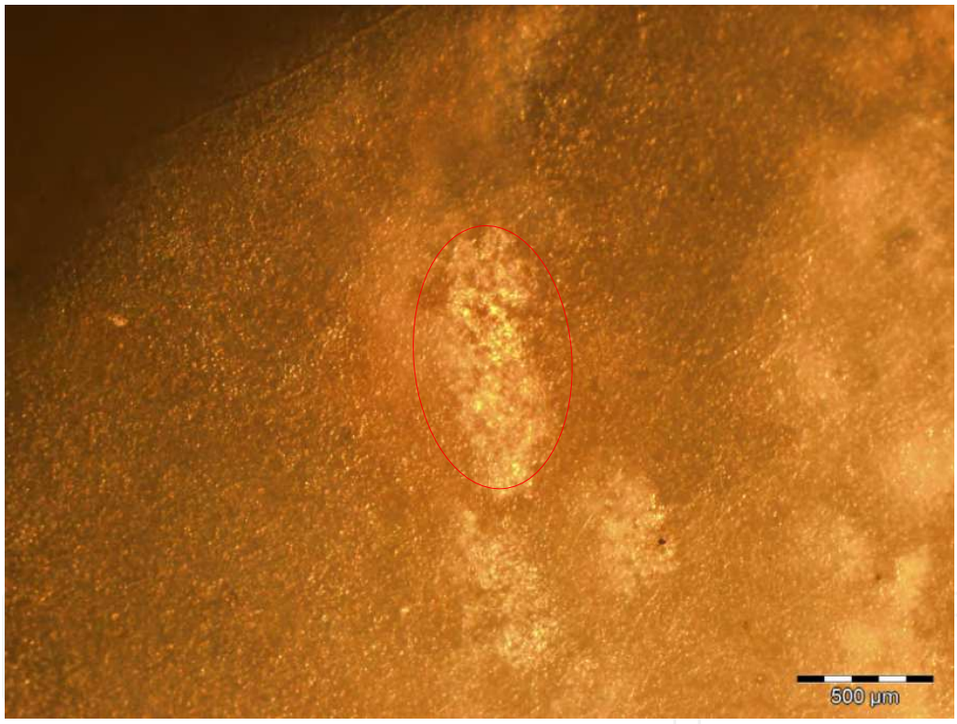

Fig. 5. The microphotograph of the sample jade-1 presents several cloudy clustering cracks sealed below the glaze surface. A few micro-cracks are open to the air (in bright sparks within the circle) in this cluster.

In fact, in terms of the OCT image, it appears to be apparent that the clustering crack is structured in an orderly fashion by an initial fractured (damaged) core and several gradually propagated micro-cracks from the core along the grain boundaries to form a considerable volume of crack body. Some branching cracks in skirts of the crack body are continuing to grow, and they sometimes joined with other branching cracks of the other crack body. Such structured clustering crack can be viewed in Figure 5a, Figure 6, and

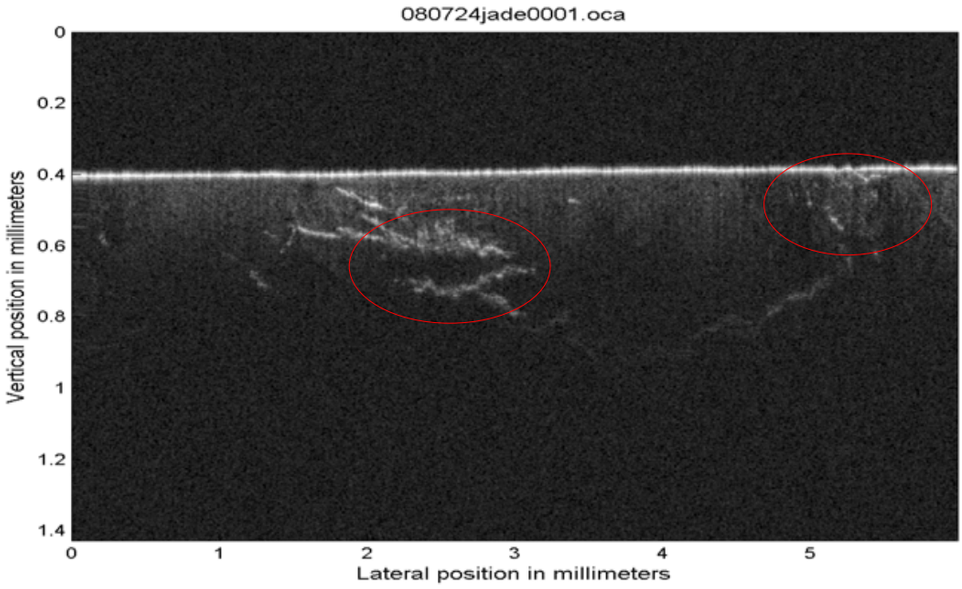

Fig. 5a. Two clustering structure cracks are presented in the image. A clustering crack usually consists of a crack body (circles) with some branching cracks that probably join other branching cracks of another crack body. The left crack presents a typical clustering structure crack in a considerable volume. The right one reveals some chips (open to the air) on the glaze surface. (image acquired by 890-nm system).

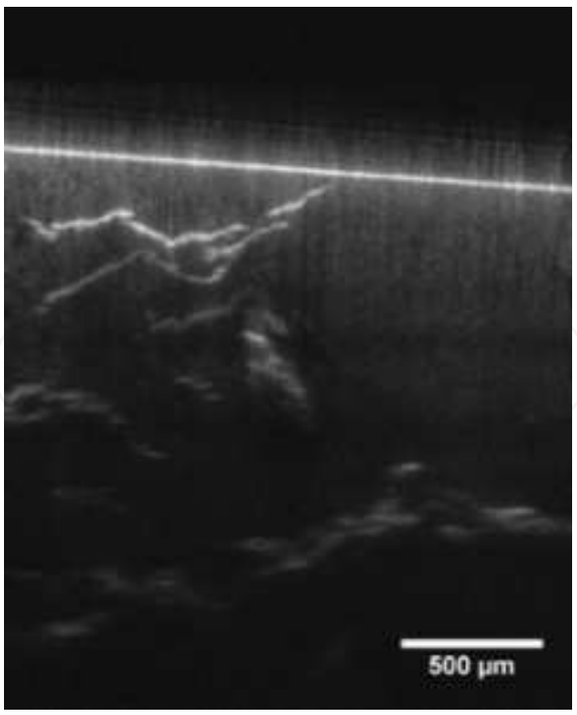

Fig. 5b. Several clustering structure cracks are presented in a tight space in the sample jade-1. (image acquired by 855-nm, focus-tracking system).

Figure 7b (circles). Moreover, when branching cracks join together among crack bodies, they should create a more complicated macrostructure in a jade material, as displayed in Figure 5b and 7a.

In contrast with Figure 5a and Figure 6, Figure 7 presents an uneven gray scale in the OCT image that implies the jade material, sample jade-3, contained several impurities. However, clustering structure cracks of various sizes are sealed in a deeper position below the surface of the sample. These complicated clustering structure cracks are exhibited more clearly in Figure 7a.

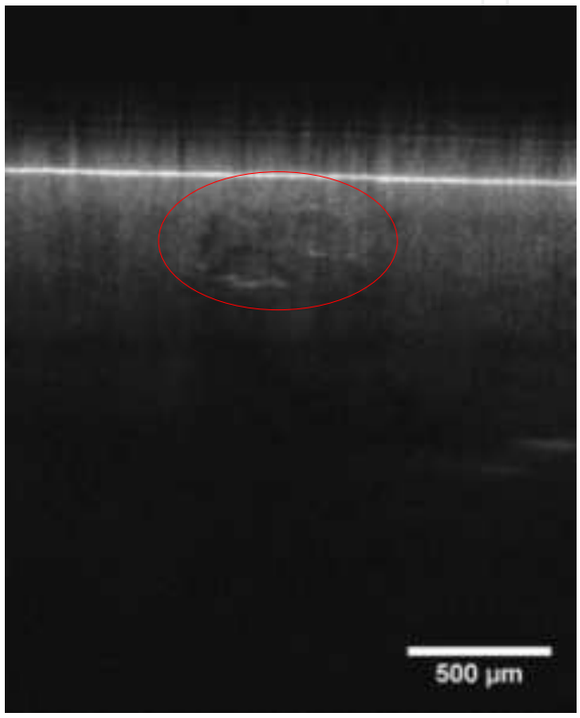

Fig. 5c. Some damage to the texture of local matrix is presented in the image of the sample jade-1. (image acquired by focus-tracking system).

4.2 Linear structure crack in jade

Figure 8 presents an extremely pure nephrite matrix of the sample jade-4 in an even and light gray scale. A 'U' shape crack is displayed in the image. Chips at the openings of this crack are revealed on the surface. This crack propagated its path in zigzag form. Figure 8-1 presents the same crack growing in an almost horizontal direction with the surface of this jade. However, the terminal tip of this crack isn't clearly revealed.

Figure 7b displays three cracks in the sample glaze-3. The left two are not open to the air, whereas the right one is open to the air with a couple of chips on the surface. However, based on the OCT images, the linear structure cracks in jade-3 and jade-4 appear to be broader and brighter than the former glaze cracks due to iron oxides deposits caused by corrosion along the crack gap in these jade samples.

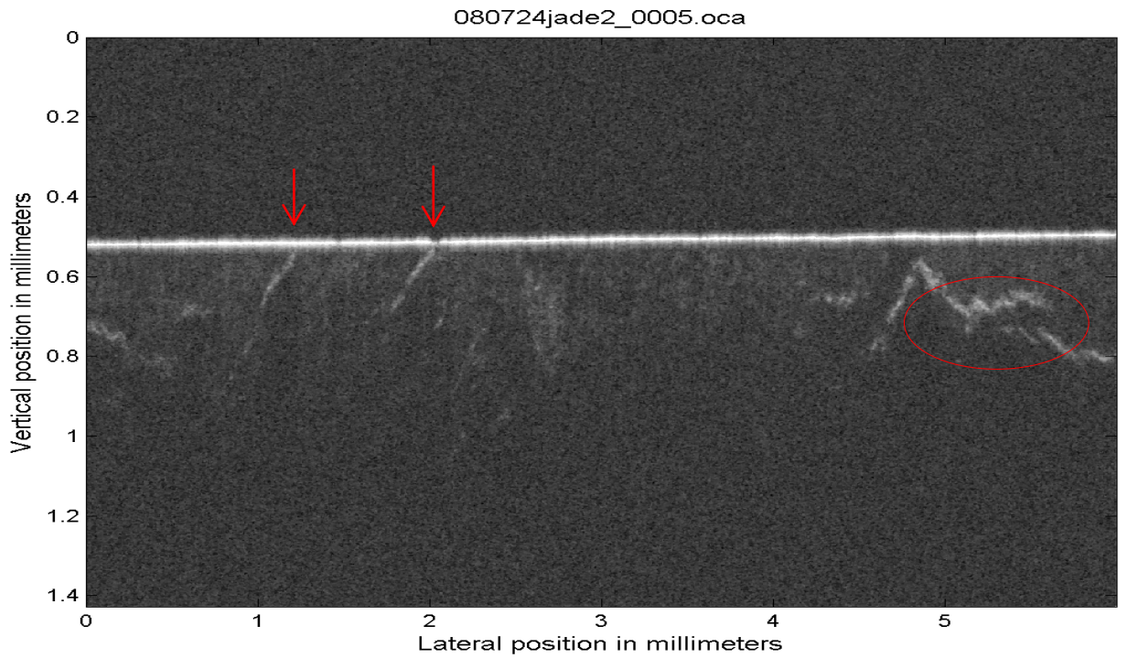

Fig. 6. A clustering structure crack is displayed on the right of the image of the sample jade-2. The circle marks the same structure crack as the one in the left circle of Figure 5a. The left arrows points to two thin linear cracks. (image acquired by 890-nm system).

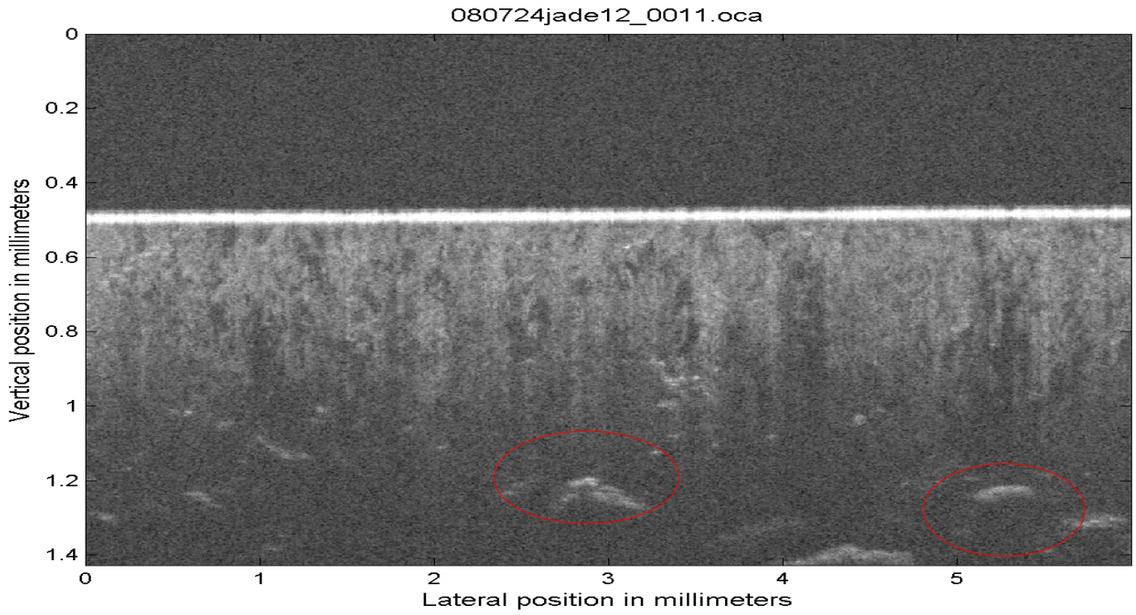

Fig. 7. Several sealed clustering structure cracks (circles) are presented in the image of sample jade-3. However, the jade matrix seems to contain rich impurities (the bright and black nodules). (image acquired by 890-nm system).

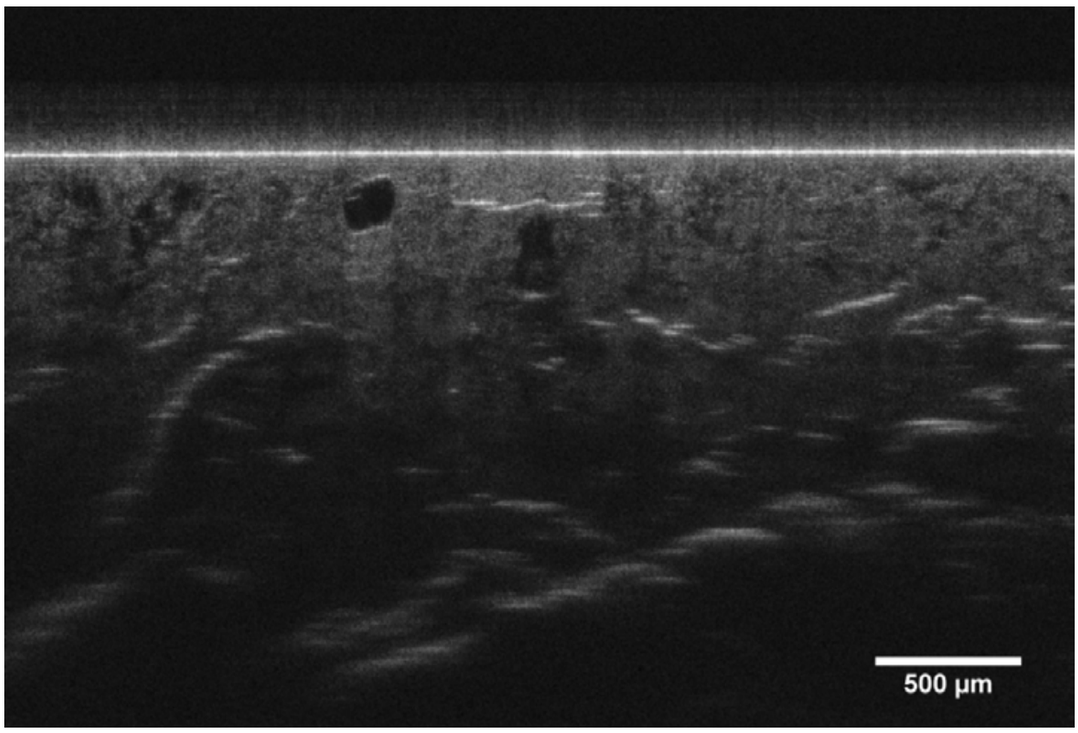

Fig. 7a. A detailed image presents considerably confused clustering and linear structure cracks with rich impurities in the sample jade-3. The imaging depth is over 2-mm in the sample. (image acquired by 855-nm, focus-tracking system).

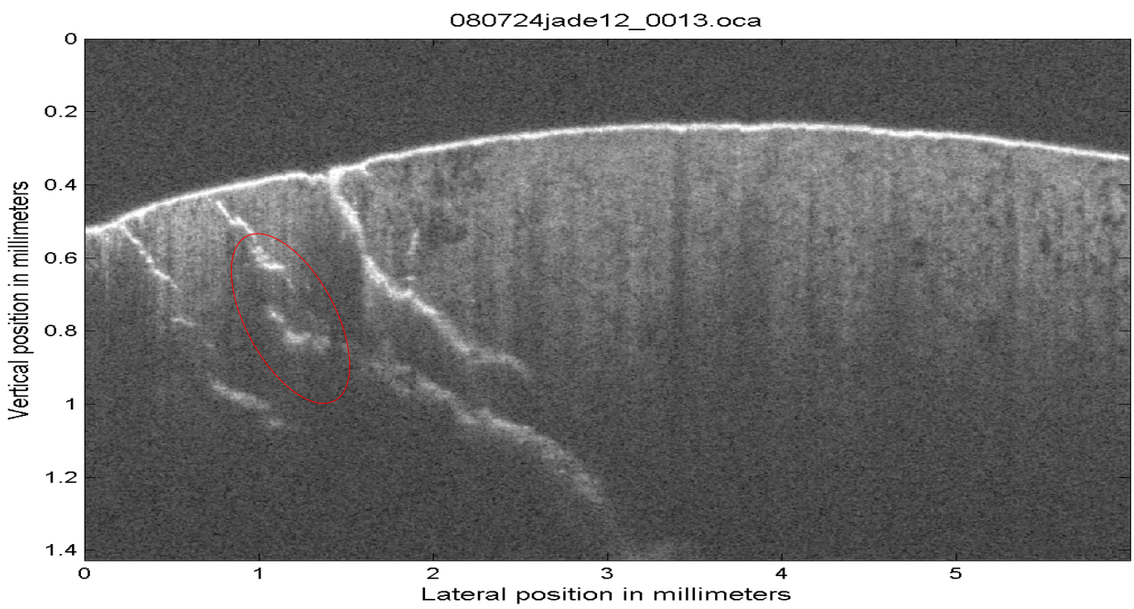

Fig. 7b. Three cracks are presented in the image of jade-3. The right one seems to be a linear structure. The other two are clustering structure cracks. The circle marks off a probable crack body of the clustering structure crack. (image acquired by 890-nm system)

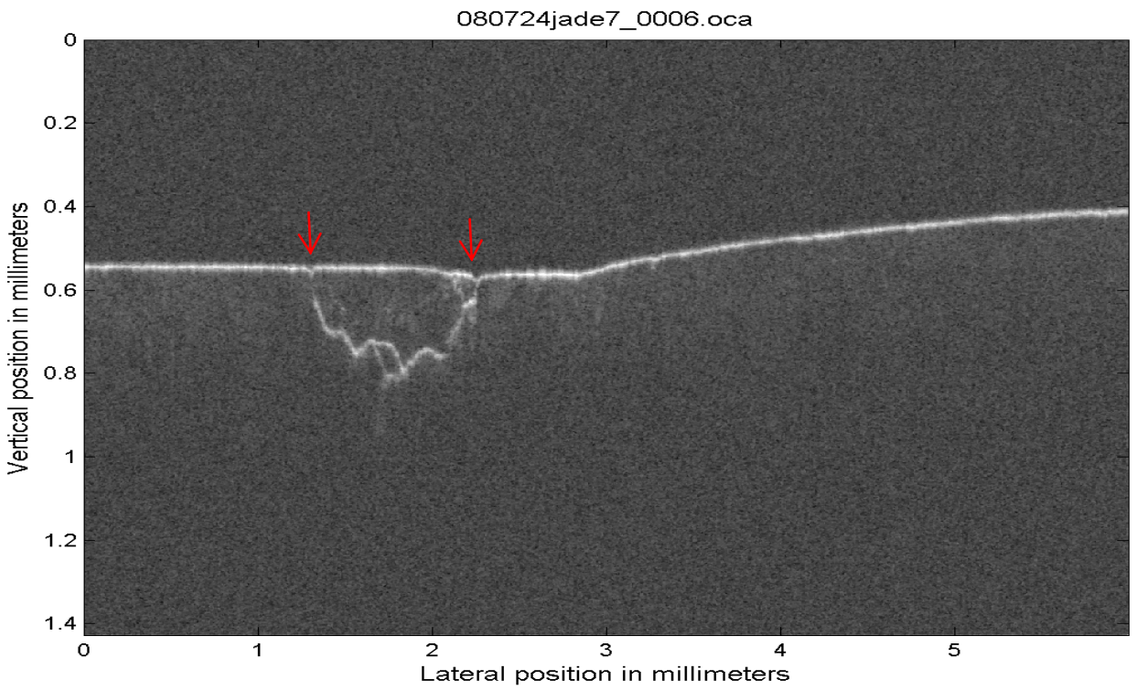

Fig. 8. A linear structure crack is presented in the image of the jade (nephrite) pebble. Some chips are revealed on the pebble's surface (arrows). The crack path propagated in zigzag form. (image acquired by 890-nm system).

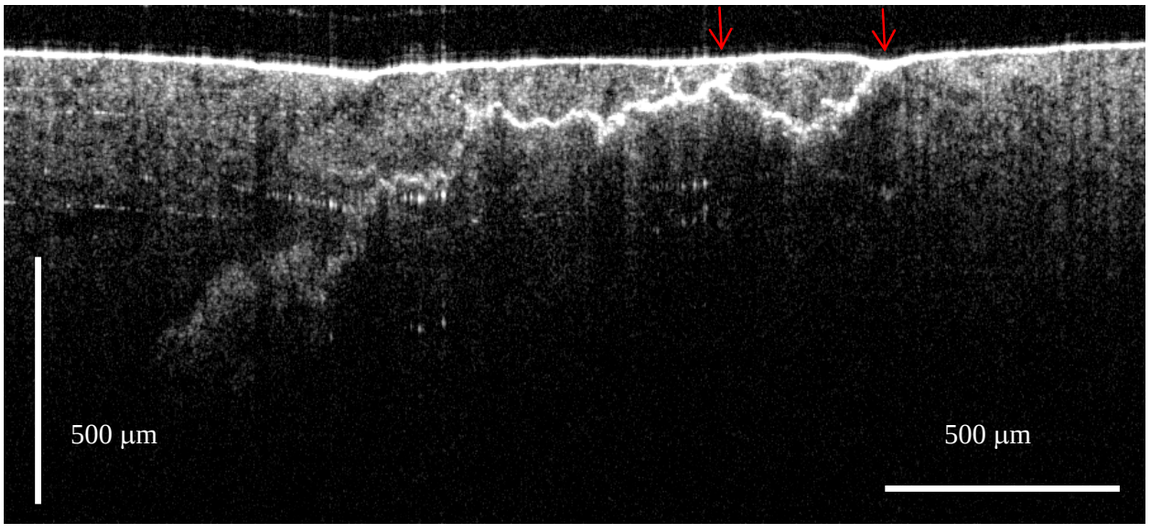

Fig. 8-1. Due to corrosion (iron oxidation) along the crack gap, the irregular or zigzag path appears to be brighter in the OCT image. The terminal tip of the crack is not clear. Two arrows indicate the same openings presented in Fig. 8. (image acquired by 930-nm system).

In addition, some thin and short linear cracks are presented in Figure 6. Two very thin cracks (left two arrows) are similar to 'T' structure crack in the glaze samples with an inclining angle of around 45 degrees. The right one reveals its opening in a small chip on the surface, whereas the left one is not open to the air. The thinness and shortness of the two cracks seem to imply the driving force for continued crack propagation in them is weak.

4.3 Discussion of the characteristics of crack morphology in jade

The characteristics of the clustering structure crack in the jade material are likely to be summarized as: (1) its basic structure is a crack body formed by many micro-cracks in clusters, with some branching cracks in skirts of the crack body; (2) some branching cracks have joined together among crack bodies to form a complicated and considerable macrostructure network; (3) most cracks are not open to the air; and (4) no clear terminal tip is revealed.

In fact, most clustering structure cracks are initiated by damage to the local texture of the jade matrix. Sometimes the damage did not expand or deteriorate in the material, and it remained for a lengthy period, as displayed in Figure 5c (circle). However, once the micro-cracks begin propagating from the damage site, the crack develops along the grain boundaries in the jade. Therefore, regardless of whether the crack has a clustering structure or linear structure, unlike most glazes' smooth path, the jades' crack path is usually in irregular or zigzag form.

However, for some thin and short cracks, such as those in Figure 6, there may be a logical interpretation. Because the sample jade-2 (Figure 6) was used by ancient peoples as a tool (Yang, 2003), these thin cracks are probably due to that function. Under an imposed stress by the force of a human arm for routine work in a non-metal ancient society, small and thin cracks were propagated within the material, as presented in the image.

5. Conclusion

The focus-tracking system is a forceful tool for imaging deeper microstructure in jade or glaze materials, with over 2-mm of depth visualized. For exploring the sealed cracks inside jade material, it is suitable. In contrast, the 890-nm system presents a detail structure of cracks in a shallower position from the surface of the sample. However, the 930-nm system should be the most effective tool to highlight the crack structure within a multi-phase inhomogeneous glaze material. With a handheld probe, a portable tool, it can be applied directly to the surface of an artifact or artwork and to rapidly acquire appropriate images. However, scanning at different positions of a crack probably obtains different information related to the same crack. It enhances the advanced 3-dimension imaging to obtain more complete information related to the cracks.

In terms of OCT demonstrating crack morphology of glaze and jade materials, it not only reveals the basic structure characteristics, but also provides quantitative research about crack variation, such as the inclining angles from the typical 'T' structure or the depth of crack. Moreover, it is also likely to offer a more scientific classification of crack in ceramic or jade materials. Although crack in brittle materials is always a difficult issue to clarify, especially the mechanism of crazing related to the thermal stress and thermal shock (Andersson & Rowcliffe, 1996; Bertsch et al., 1974; Hasselman, 1969; Clarke et al., 1966),

establishing the structure of crack and the relationship between crack and local components would make an important contribution to advanced scientific research.

In addition, the present result also contributes to art history study, especially in verifying certain Chinese historical records. For instance, according to ancient Chinese texts, some Southern Song (AD 1127-1279) Guan wares were dyed using eel blood to make the crack line is dark brown (Gao, 1591). However, based on the present research, several cracks are not open to the air, thus, the dyed eel blood legend seems to become more fancifully. Moreover, with regard to specific endowed artistic attributes of crack patterns in glaze, the research also provides a logical and scientific interpretation for their unique and subtle visual effect.

6. Acknowledgment

The author thanks Prof. Vandiver for providing a Ru shard sample (the present glaze-3) and Ms. Carol Elliott for her English editing suggestions.

7. References

Andersson, Tomas & Rowcliffe, David J. (1996). Indentation thermal shock test for ceramics. *Journal of the American Ceramic Society*, 79, 6, pp. 1509-1514, ISSN 0002-7820

Bertsch, B. E.; Larson, D. R. & Hasselman, D. P. H. (1974). Effect of crack density on strength loss of polycrystalline Al_2O_3 subjected to severe thermal shock. *Journal of the American Ceramic Society – Discussions and Notes*, 57, 5, pp. 235-236, ISSN 0002-7820

Bradt, Richard C.; Newnham, Robert E. & Biggers, J. V. (1973). The toughness of jade. *American Mineralogist*, 58, 7 & 8, pp. 727-732, ISSN 0003-004X

Chang, Shoude; Mao, Youxin; Chang, Guangming & Flueraru, Costel. (2010). Optical Coherence Tomography used for jade industry. *Proc. of SPIE*, 7855 785514, pp. 1-9, ISSN 1996-756X (web)

Clarke, F. J. P.; Tattersall, H. G. & Tappin, G. (1966). Toughness of ceramics and their work of fracture. *Proceedings of the British Ceramic Society*, 6, pp. 163-172, ISSN 0524-5141

Coble, R. L. & Kingery, W. D. (1955). Effect of porosity on thermal stress fracture. *Journal of the American Ceramic Society*, 38, 1, pp. 33-37, ISSN 0002-7820

Coppola, J. A. & Bradt, R. C. (1972). Measurement of fracture surface energy of SiC. *Journal of the American Ceramic Society*, 55, 9, pp. 455-460, ISSN 0002-7820

Elias, Mady; Magnain, Caroline & Frigerio, Jean Marc. (2010). Contribution of surface state characterization to studies of works of art. *Applied Optics*, 49, 11, pp. 2151-2160, ISSN 1559-128X

Faber, K. T.; Huang, M. D. & Evans, A. G. (1981). Quantitative studies of thermal shock in ceramics based on a novel test technique. *Journal of the American Ceramic Society*, 64, 5, pp. 296-301, ISSN 0002-7820

Friedman, M.; Handid, J. & Alani, G. (1972). Fracture-surface energy of rocks. *International Journal of Rock Mechanics and Mining Sciences*, 9, pp. 757-766, ISSN 0020-7624

Gao, Lian. (1591). *Ya Shang Zhai Zun Sheng Ba Jian (雅尚齋遵生八牋)*, Shu Mu Wen Xian Chu Ban She, ISBN 7-5013-0586-2, Beijing.

Hasselman, D. P. H. (1969). Griffith criterion and thermal shock resistance of single-phase versus multiphase brittle ceramics. *Journal of the American Ceramic Society – Discussions and Notes*, 52, 5, pp. 288-289, ISSN 0002-7820

Hasselman, D. P. H. (1969). Unified theory of thermal shock fracture initiation and crack propagation in brittle ceramics. *Journal of the American Ceramic Society*, 52, 11, pp. 600-604, ISSN 0002-7820

Kingery, W. D.; Bowen, H. K. & Uhlmann, D. R. (1976). *Introduction to Ceramics (Second Edition),* p. 550, John Wiley & Sons, ISBN 0471478601, New York.

Klein, Justin; Winkler, Amy M.; Yang, M.-L.; Tumlinson, Alex & Barton, Jennifer K. (2011). Quantitative bubble imaging in ceramic glazes using a custom algorithm and focus-tracking optical coherence tomography. (forthcoming)

Li, Fenggong. (1925). *Yu Ya (玉雅)*, in *Gu Yu Kao Shi Jian Shang Cong Bian*, pp. 941-1046, Shu Mu Wen Xian Chu Ban She, ISBN 7-5013-0962-0, Beijing.

Liang, Haida; Peric, Borislava; Hughes, Michael; Podoleanu, Adrian; Spring, Marika & Roehrs, Stefan. (2008). Optical Coherence Tomography in archaeological and conservation science – a new emerging field. *Proc. of SPIE*, 7139 713915, pp. 1-9, ISSN 1996-756X (web)

Norton, F. H. (1952). *Elements of Ceramics*, Addison-Wesley, Cambridge.

Palmer, J. P. (1967). *Jade*, pp. 13-19, Spring Books, London.

Schurecht, H. G. & Fuller, D. H. (1931). Some effects of thermal shock in causing crazing of glazed ceramic ware. *Journal of the American Ceramic Society,* 14, 8, pp. 565-571, ISSN 0002-7820

Schurecht, H. G. & Pole, G. R. (1932). Some special types of crazing. *Journal of the American Ceramic Society,* 15, 11, pp. 632-637, ISSN 0002-7820

Seaton, C. C. & Dutta, S. K. (1974). Effect of grain size on crack propagation in thermally shocked B_4C. *Journal of the American Ceramic Society—Discussions and Notes*, 57, 5, pp. 228-229, ISSN 0002-7820

Shaw, Kenneth. (1971). *Ceramic Glazes,* pp. 128-129, Elsevier Publishing Company Limited, ISBN 0444201076, Amsterdam.

Simmons, Joseph. (1977). Refractive index and density changes in a phase-separated Borosilicate glass. *Journal of Non-Crystalline Solids*, 24, pp. 77-88, ISSN 0022-3093

Targowski, Piotr. (2008). Publications, In: *Optical Coherence Tomography for Examination of Objects of Art*, August 1, 2011, Available from: http://www.oct4art.eu/

THORLABS. (2011). Spectral Radar OCT system. *Microscopy and laser imaging,* August 1, 2011, Available from: http://www.thorlabs.com/catalogPages/595.pdf

Whitlock, Herbert P. & Ehrmann, Martin L. (1949). *The Story of Jade*, Sheridan House, New York.

Winkler, A. M.; Rice, P. F.; Drezek, R. A & Barton, J. K. (2010). Quantitative tool for rapid disease mapping using optical coherence tomography images of azoxymethane treated mouse colon. *Journal of Biomedical Optics*, 15, 4, 041512, ISSN 1083-3668

Yang, M.–L.; Winkler, Amy M.; Klein, Justin & Barton, Jennifer K. (2012). Using Optical Coherence Tomography to characterize thick-glaze structure: Chinese Southern Song Guan glaze case study. *Studies in Conservation,* 57, 1, ISSN 0039-3630 (publishing)

Yang, M.-L.; Winkler, Amy M.; Barton, Jennifer K. & Vandiver, Pamela B. (2009). Using Optical Coherence Tomography to examine the subsurface morphology of Chinese glazes. *Archaeometry* 51, 5, pp. 808-821, ISSN 0003-813X

Yang, M.-L.; Lu, C.-W.; Hsu, I.-J. & Yang, C. C. (2004). The use of Optical Coherence Tomography for monitoring the subsurface morphologies of archaic jades. *Archaeometry*, 46, 2, pp. 171-182, ISSN 0003-813X

Yang, Mei-Li. (2003). *The Story of Stone Tools: Special Exhibition of Stone Artifacts Donated by Lin Yao-chen*, the National Palace Museum, ISBN 957-562-448-3, Teipei.

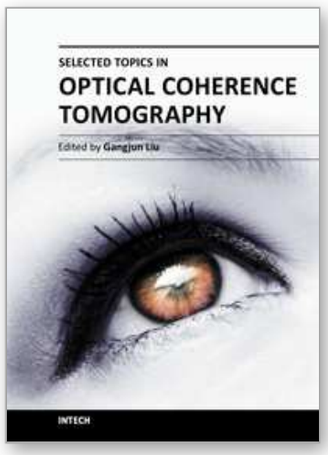

Selected Topics in Optical Coherence Tomography

Edited by Dr. Gangjun Liu

ISBN 978-953-51-0034-8
Hard cover, 280 pages
Publisher InTech
Published online 08, February, 2012
Published in print edition February, 2012

This book includes different exciting topics in the OCT fields, written by experts from all over the world. Technological developments, as well as clinical and industrial applications are covered. Some interesting topics like the ultrahigh resolution OCT, the functional extension of OCT and the full field OCT are reviewed, and the applications of OCT in ophthalmology, cardiology and dentistry are also addressed. I believe that a broad range of readers, such as students, researchers and physicians will benefit from this book.

InTech Europe
University Campus STeP Ri
Slavka Krautzeka 83/A
51000 Rijeka, Croatia
Phone: +385 (51) 770 447
Fax: +385 (51) 686 166
www.intechopen.com

InTech China
Unit 405, Office Block, Hotel Equatorial Shanghai
No.65, Yan An Road (West), Shanghai, 200040, China
中国上海市延安西路65号上海国际贵都大饭店办公楼405单元
Phone: +86-21-62489820
Fax: +86-21-62489821

IntechOpen